Monthly Notices of the ROYAL ASTRONOMICAL SOCIETY

MNRAS **509,** 1252–1261 (2022) https://doi.org/10.1093/mnras/stab3015
Advance Access publication 2021 October 20

Rotational excitation of H_3O^+ cations by *para*-H_2: improved collisional data at low temperatures

Sándor Demes [1★], François Lique,[1★] Alexandre Faure [2★], Floris F. S. van der Tak,[3★] Claire Rist[2] and Pierre Hily-Blant [2]

[1] *Univ Rennes, CNRS, IPR (Institut de Physique de Rennes) - UMR 6251, F-35000 Rennes, France*
[2] *IPAG, Université Grenoble Alpes and CNRS, CS 40700, F-38058 Grenoble, France*
[3] *SRON Netherlands Institute for Space Research and Kapteyn Astronomical Institute, University of Groningen, NL-9747 AD Groningen, The Netherlands*

Accepted 2021 October 14. Received 2021 September 28; in original form 2021 June 23

ABSTRACT

The hydronium cation plays a crucial role in interstellar oxygen and water chemistry. While its spectroscopy was extensively investigated earlier, the collisional excitation of H_3O^+ is not well studied yet. In this work, we present state-to-state collisional data for the rotational de-excitation of both *ortho*- and *para*-H_3O^+ due to *para*-H_2 impact. The cross sections are calculated within the close-coupling formalism using our recent, highly accurate, rigid-rotor potential energy surface for this collision system. The corresponding thermal rate coefficients are computed up to 100 K. For *para*-H_3O^+, the lowest 20 rotation-inversion states were considered in the calculations, while for *ortho*-H_3O^+, the lowest 11 states are involved (up to $j \leq 5$), so all levels with rotational energy below 420 K (292 cm^{-1}) are studied. In order to analyse the impact of the new collisional rate coefficients on the excitation of H_3O^+ in astrophysical environments, radiative transfer calculations are also provided. The most relevant emission lines from an astrophysical point of view are studied, taking into account the transitions at 307, 365, 389, and 396 GHz. We show that our new collisional data have a non-negligible impact (from a few per cents up to about a factor of 3) on the brightness and excitation temperatures of H_3O^+, justifying the revision of the physical conditions in the appropriate astrophysical observations. The calculated rate coefficients allow one to recalculate the column density of hydronium in interstellar clouds, which can lead to a better understanding of interstellar water and oxygen chemistry.

Key words: astrochemistry – molecular processes – radiative transfer – scattering – methods: laboratory: molecular – ISM: molecules.

1 INTRODUCTION

It was shown earlier by Herbst & Klemperer (1973), Phillips, van Dishoeck & Keene (1992), Sternberg & Dalgarno (1995), and van der Tak, Aalto & Meijerink (2008) that hydronium cation H_3O^+ is a very important chemical species in interstellar ion-molecule reaction schemes. It is present both in dense and diffuse interstellar medium (ISM) playing a very important role in oxygen and water chemistry (Sternberg & Dalgarno 1995; Goicoechea & Cernicharo 2001; Gerin et al. 2010; González-Alfonso et al. 2013; van Dishoeck, Herbst & Neufeld 2013). According to Hollenbach et al. (2012), the formation of H_3O^+ proceeds via two different ways in low-temperature diffuse and dense molecular clouds (see also van Dishoeck et al. 2013). In diffuse clouds as well as near the surfaces of molecular clouds, the following reactions take place

$$\begin{aligned} &\text{(a)}\ OH^+ + H_2 \rightarrow H_2O^+ + H, \\ &\text{(b)}\ H_2O^+ + H_2 \rightarrow H_3O^+ + H. \end{aligned} \quad (1)$$

Here, the OH^+ cations are formed by an 'atomic' route via the interaction of O^+ ions with H_2, where the oxygen ions are produced in $H^+ + O$ reaction.

Deeper in the opaque interiors of molecular clouds, the formation of H_3O^+ can take place also via reactions (a) and (b) defined in equation (1). In this region however, both OH^+ and H_2O^+ cations can be produced directly from H_3^+ through interaction with oxygen atoms, so reaction (a) could be skipped. H^+ and H_3^+ ions needed for H_3O^+ formation are provided by cosmic ray ionization of H_2. In our Galaxy, this process proceeds at a rate of $10^{-17} - 10^{-15}$ s^{-1}, depending on cloud density and Galactocentric radius (van der Tak & Van Dishoeck 2000; Indriolo et al. 2015). The relative abundances of H_2O and H_3O^+ have been used to constrain the ionization rates of molecular clouds in external galaxies (van der Tak et al. 2016).

The dissociative recombination of H_3O^+ leads to the formation of neutral OH and H_2O products, where the hydroxyl radical can react with oxygen atoms afterwards in order to form O_2 molecules (Vejby-Christensen et al. 1997; Jensen et al. 2000; Yu et al. 2009; Zhaunerchyk et al. 2009). H_3O^+ is not only the backbone of interstellar oxygen chemistry, but it is also one of the most important cations in all branches of chemistry in general (Mann et al. 2013; Yu & Bowman 2016), which is intensively studied in many aspects. As we mentioned in our recent work (Demes et al. 2020, referred

★ E-mail: sandor.demes@univ-rennes1.fr (SD); francois.lique@univ-rennes1.fr (FL); alexandre.faure@univ-grenoble-alpes.fr (AF); f.f.s.van.der.tak@sron.nl (FFSvdT)

as Paper I hereafter), finding the abundance of H_3O^+ cations can be used as an indirect way of determining the abundance of interstellar water (Phillips et al. 1992). In order to understand the role of hydronium cations in astrophysical media, however, the features of both its radiative and collisional excitation should be studied. Numerous high-resolution spectroscopy measurements were carried out for H_3O^+, which were collected by Yu et al. (2009), while Yurchenko et al. (2020) theoretically studied its ro-vibrational levels recently. The electron-impact excitation of H_3O^+ was studied by Faure & Tennyson (2003), who combined the **R**-matrix theory with the adiabatic-nuclei-rotation approximation. Unfortunately, there are only limited works devoted to its collisions with interstellar atoms and molecules. For example, for rotational excitation of H_3O^+ by molecular hydrogen (which is the most abundant molecule in the ISM) only approximated, scaled data are available in the literature (Offer & van Hemert 1992), which are only accurate to order of magnitude (see the review by van der Tak et al. 2020 for a discussion of the accuracy of scaled collision data). So reliable and precise rate coefficients are obviously needed for describing the collisional excitation of H_3O^+ in order to interpret the astrophysical observations in the ISM.

In the first rotational excitation study by Offer & van Hemert (1992), the H_3O^+–H_2 collision was modelled with a scaled interaction potential of the isoelectronic NH_3 molecule (in collision with H_2), taking into account its electronic and geometrical properties along with the large 'umbrella' inversion splitting constant. Both the *para*(*p*)- and *ortho*(*o*)-H_3O^+ nuclear spin isomers were studied in collision with ground-state *para*- and *ortho*-H_2. In order to improve the model potential energy surface (PES) based on NH_3–H_2 interaction, the authors added a long-range correction calculated by second-order perturbation theory, fitted by analytical functions. However, even with this correction included the model cannot correctly describe the ionic nature of H_3O^+, so the cross-section data obtained by Offer & van Hemert (1992) should be improved and recalculated using a more accurate PES. It is also worth noting that the authors provide converged state-to-state data only for the *p*-H_3O^+ − *p*-H_2 collision for a single collision energy (101 cm^{-1}), while for the *o*-H_3O^+ − *p*-H_2 and *p*-H_3O^+ − *o*-H_2 interactions they only performed benchmark calculations with a very limited number of partial waves $J = 0 - 2$ (where J is the total angular momentum).

The collisional excitation of H_3O^+ by He atoms (as a template for H_2) was recently studied by El Hanini et al. (2019). Helium is, however, by a factor of 5 less abundant than H_2. Rotational excitation cross sections were computed by means of the close coupling or coupled channel (CC) method by the authors up to 500 cm^{-1} collision energies in case of *o*-H_3O^+, and up to 300 cm^{-1} in case of *p*-H_3O^+, while the thermal rate coefficients were calculated up to 50 K. They used a three-dimensional (3D) PES with fixed intramolecular distances for both colliding partners, calculated by the coupled-cluster theory at the level of single, double, and perturbative corrections for triple excitations [CCSD(T)] and with a non-standard valence quadruple-zeta (AVQZ) basis set. The inversion splitting effects were neglected in the work, which is questionable in case of the H_3O^+ cation because of its rather large (∼55 cm^{-1}) inversion splitting constant (Yu et al. 2009). The global well depth of the H_3O^+–He system, as it was calculated by the authors taking into account the basis set superposition error (BSSE) corrections, is about 354.53 cm^{-1}. As it was shown by Roueff & Lique (2013), significant differences could be observed between the rate coefficients for collisions with He and H_2. According to this, new, reliable rate coefficients are obviously needed for the collision of H_3O^+ with H_2 in order to more precisely estimate its abundance from emission spectral lines observed in the ISM. Without such rates the molecular abundances could be only approximated, assuming local thermodynamic equilibrium (LTE), which is usually not a good approximation for typical interstellar conditions (Roueff & Lique 2013).

In this paper, we provide new collisional cross-section and thermal rate coefficient data for the interaction of H_3O^+ with H_2 under ISM conditions, based on our new, accurate 5D PES (Paper I). The rotational (non-spherical) structure of *p*-H_2 was taken into consideration. A detailed comparison with the available data for H_3O^+–He (El Hanini et al. 2019) and NH_3–H_2 (Bouhafs et al. 2017) collisions is presented. As a first astrophysical application, in order to illustrate the influence of our new rate coefficients on astrophysical modelling, we also perform radiative transfer calculations to analyse the collisional excitation of H_3O^+ in interstellar molecular clouds.

The paper is organized as follows: In Section 2, the details of the PES as well as the scattering and radiative transfer calculations are presented. We report state-to-state cross sections and rate coefficients for the rotational de-excitation of H_3O^+ by H_2 in Section 3, where in subsection 3.3, we also present the results of radiative transfer calculation. Our concluding remarks are drawn in Section 4.

2 METHODS

2.1 Potential energy surface

We have used our recent 5D rigid-rotor PES (Paper I) to model the collisional dynamics of the H_3O^+–H_2 system. The PES was calculated using the explicitly correlated coupled-cluster theory at the level of singles and doubles with perturbative corrections for triple excitations [CCSD(T)-F12] with the moderate-size augmented correlation-consistent valence triple zeta (aug-cc-pVTZ) basis set and applying the counterpoise procedure of Boys & Bernardi (1970) in order to eliminate the effects of BSSE (see Paper I for full details).

We used a Jacobi coordinate system to define the geometry of the H_3O^+–H_2 system. The centre of the coordinate system is chosen to be in the centre of mass (c.o.m.) of the H_3O^+ cation (i.e. molecular frame representation). A single radial parameter R defines the intermolecular distance between the c.o.m. of H_3O^+ and H_2, θ, and ϕ spherical angles characterize the angular position of H_2 relative to the centre of the coordinate system, while two additional angles define the orientation of the H_2 molecule. We used the rigid rotor approximation in order to reduce the dimensionality. It should be noted that the inversion frequency of H_3O^+ is much larger than that of NH_3, however, as Offer & van Hemert (1992) have shown the explicit inclusion of the inversion motion has only a small impact on the rotational cross sections, so that the rigid-rotor approximation is valid and reasonable for our case. For the H_2 molecule, we applied a bond length of $r_{H-H} = 1.44874$ bohr, calculated by Bubin & Adamowicz (2003), while for the H_3O^+ cation, the experimental structural data of Tang & Oka (1999) was used: $r_{O-H} = 1.8406$ bohr for the bond lengths and $\alpha_{H-O-H} = 113.^{\circ}6$ for the bond angles. At each intermolecular distance R, the interaction energy was fitted using a least square standard linear method. All significant analytical terms were selected iteratively, using a Monte Carlo error estimator described by Rist & Faure (2012), resulting in a final set of 208 expansion functions with anisotropies up to $l_1 = 16$ and $l_2 = 4$ (the l_1 and l_2 indices refer to the tensor ranks of the angular dependence of the H_3O^+ and H_2 orientations, respectively). The root mean square

Table 1. List of the rotational energy levels for *ortho-* and *para*-H_3O^+, which were considered in collisional studies of this work. The corresponding energies are taken from JPL data base (Pickett, Cohen & Drouin 2010, Species Tag: 19004, version 3, compiled by Yu & Drouin, Jan. 2010).

	para-H_3O^+			*ortho*-H_3O^+	
State Label	Rotational State j_k^ϵ	Rotational (internal) Energy (cm^{-1})	State Label	Rotational State j_k^ϵ	Rotational (internal) Energy (cm^{-1})
(1)	1_1^+	0.000	(1)	1_0^+	5.101
(2)	2_2^+	29.697	(2)	0_0^-	37.947
(3)	2_1^+	44.986	(3)	3_3^+	71.681
(4)	1_1^-	55.233	(4)	2_0^-	104.239
(5)	2_2^-	84.977	(5)	3_0^+	117.457
(6)	3_2^+	97.145	(6)	3_3^-	127.172
(7)	2_1^-	99.427	(7)	4_3^+	161.573
(8)	3_1^+	112.384	(8)	4_3^-	215.486
(9)	4_4^+	125.939	(9)	4_0^-	258.636
(10)	3_2^-	151.241	(10)	6_6^+	271.201
(11)	3_1^-	165.657	(11)	5_3^+	273.697
(12)	4_4^-	181.807			
(13)	4_2^+	186.926			
(14)	5_5^+	192.453			
(15)	4_1^+	202.099			
(16)	5_4^+	238.256			
(17)	4_2^-	239.479			
(18)	5_5^-	248.863			
(19)	4_1^-	253.850			
(20)	5_4^-	292.146			

(rms) residual was found to be lower than 1 cm^{-1} in the long-range region of the PES and also in the potential well region. The rms error on the expansion coefficients was also found to be smaller than 1 cm^{-1} in these regions of the interaction potential. The interpolation of the analytical coefficients was finally performed using a cubic spline radial interpolation scheme over the whole intermolecular distance range ($R = 4-30$ bohr), and it was smoothly connected to standard extrapolations using the switch function applied earlier by Valiron et al. (2008).

Until otherwise noted, we used the following units throughout this paper: atomic units (au) for distances (1 au = 1 bohr $\approx$ 5.29177×10^{-9} cm), and wavenumbers (cm^{-1}) for energies (1 cm^{-1} $\approx$ 1.4388 K).

2.2 Scattering calculations

We have calculated the state-to-state rotational de-excitation cross sections (σ) and thermal rate coefficients ($k(T)$) for the collision of both *ortho-* and *para*-H_3O^+ with *para*-H_2. We determined the σ up to 800 cm^{-1} total energies from a close-coupling approach using the HIBRIDON scattering code (Manolopoulos 1986; Alexander & Manolopoulos 1987). Similar calculations were performed for the isoelectronic NH_3–H_2 collision system (which is also a 'symmetric top molecule – diatom' collision system) in a broad kinetic energy range by Bouhafs et al. (2017). The rotational states involved in our calculations are denoted by j_k^ϵ, where j is the total angular momentum of the H_3O^+ cation, k is its projection on the C_3 rotational axis, and $\epsilon = \pm$ is an inversion symmetry index (for more details, see Rist, Alexander & Valiron 1993). It is worth noting that the *ortho*-H_3O^+ is characterized with $k = 3n$ quantum numbers (where $n = 0, 1, 2, \ldots$), while all other k quantum numbers (e.g. $k = 1, 2, 4, 5, \ldots$) define the H_3O^+ with *para* nuclear spin symmetry.

In the case of the hydronium cation, we used the most recent experimental rotational constants from Yu et al. (2009): B = 11.15458 cm^{-1} and C = 6.19102 cm^{-1}. The ground-state inversion splitting constant of H_3O^+ measured by Yu et al. (2009) is 55.34997 cm^{-1}, which is nearly two orders of magnitude larger than that of NH_3 (0.7903 cm^{-1}). In case of the H_2 molecule, we considered the B_{H_2} = 59.3801 cm^{-1} rotational constant, in accordance with Bouhafs et al. (2017). The reduced mass of the H_3O^+–H_2 system is found to be 1.82273 amu. Just as in Paper I, we only used a reduced 55-term expansion of our analytical PES in current scattering calculations, including anisotropies up to $l_1 \leq 6$ and $l_2 \leq 2$. The implementation of the full, 208-term angular basis into the scattering code would be technically difficult and would make the close-coupling calculations unnecessarily heavy and computationally too expensive. However, in order to study the effect of the size of the analytical potential on the cross sections, we performed benchmark calculations also with a 39-term angular basis, in which all terms with $l_1 = 6$ were removed. The results show that the 55-term angular basis we used in the calculations is enough to ensure a convergence always better than 10 − 20 per cent for any particular energy and transition considered, and generally keep the accuracy on the level of a few per cents.

We calculated the inelastic cross sections for transitions between rotational levels with internal energy $\leq$420 K (292 cm^{-1}). The complete set of these rotational levels for both *ortho-* and *para*-H_3O^+ are shown in Table 1. The basis set size (j_{max}) along with the maximum total angular momentum (J_{tot}) were selected depending on the collision energy. Their particular values were found following preliminary convergence test calculations with a convergence threshold criteria of 1 and 0.01 per cent mean deviations, respectively. In order to adequately describe the resonances in the cross sections, a very small energy step size (E_{step}) was chosen at low collision energies (0.1 cm^{-1}), which was then gradually increased (until 5 cm^{-1} at high energies). The values of j_{max}, J_{tot}, and E_{step} parameters used in the calculations for the particular collision energy intervals (from E_{init} to E_{fin}) are listed in Table 2. It is worth mentioning that the j_{max} parameter refers only to the rotational basis used for the

Table 2. A full list of the basis set size (j_{max}) and maximum total angular momentum (J_{tot}) parameters, which were found by systematic convergence tests for the particular total energy intervals. The step size for the energies (E_{step}) used in the computations are also listed.

ortho-H_3O^+−*para*-H_2 collision					*para*-H_3O^+−*para*-H_2 collision				
E_{init} (cm^{-1})	E_{fin} (cm^{-1})	E_{step} (cm^{-1})	j_{max}	J_{tot}	E_{init} (cm^{-1})	E_{fin} (cm^{-1})	E_{step} (cm^{-1})	j_{max}	J_{tot}
55.4	99.9	0.1	9	23	47.1	74.9	0.1	17	18
100	149.9	0.1	9	30	75	99.9	0.1	17	22
150	174.5	0.5	9	34	100	124.9	0.1	17	26
175	199.5	0.5	9	35	125	149.9	0.1	17	30
200	224.5	0.5	10	42	150	174.5	0.5	17	34
225	249.5	0.5	10	43	175	199.5	0.5	17	38
250	349.5	0.5	10	50	200	224	1	17	39
350	374.5	0.5	10	51	225	249	1	17	43
375	399.5	0.5	10	55	250	274	1	17	44
400	424.5	0.5	10	56	275	299	1	17	48
425	449.5	0.5	12	57	300	324	1	17	49
450	474.5	0.5	12	58	325	374	1	17	51
475	499.5	0.5	12	60	375	399	1	17	52
500	508	2	12	73	400	424	1	17	53
510	522.5	2.5	12	73	425	449	1	17	54
525	547.5	2.5	12	74	450	474	1	17	55
550	570	5	12	74	475	499	1	17	56
575	620	5	12	79	500	518.75	1.25	17	58
625	645	5	12	81	520	547.5	2.5	17	58
650	670	5	12	82	550	570	5	17	59
675	695	5	12	83	575	620	5	17	60
700	720	5	13	84	625	695	5	16	62
725	745	5	13	85	700	745	5	16	63
750	770	5	13	87	750	800	5	16	65
775	800	5	13	93					

H_3O^+ cation. For *para*-H_2, the two lowest even rotational states were taken into account in the scattering calculations, i.e. $j_{H_2} = 0, 2$.

The calculated cross sections allow to determine the rate coefficients up to 100 K kinetic temperatures by integrating over a Maxwell–Boltzmann distribution of relative velocities (Le Picard et al. 2019)

$$k_{i\to f}(T) = \left(\frac{8}{\pi\mu k_B^3 T^3}\right)^{\frac{1}{2}} \int_0^\infty \sigma_{i\to f} E_c e^{-\frac{E_c}{k_B T}} dE_c, \quad (2)$$

where E_c is the collision energy, $\sigma_{i\to f}$ is the cross-section for transition from the initial state (i) to the final state (f), μ is the reduced mass of the system, and k_B is the Boltzmann constant.

2.3 Radiative transfer calculations

Using the new set of collisional rate coefficients, radiative transfer calculations were performed in order to determine the T_R radiance and T_{exc} excitation temperatures as well as the τ opacity (optical depth) parameters for radiative transitions of *ortho*- and *para*-H_3O^+ under specific interstellar physical conditions. The calculations were performed using the latest version of the RADEX non-LTE radiative transfer computer programme (van der Tak et al. 2007). In order to solve the radiative transfer equation, the uniform sphere escape probability method has been applied. In the calculations, the physical conditions were either systematically varied or constrained. For example, the *para*-H_2 molecular densities were considered in the interval of $n(H_2) = 10^3 - 10^{12}$ cm^{-3}, the molecular column density N was varied from 1×10^{12} up to 1×10^{15} cm^{-2}, while the calculated rate coefficients allowed one to explore a kinetic energy range up to $T_{kin} = 100$ K. The background radiation temperature and the FWHM line width parameters were kept fixed in all calculations at $T_{bg} = 2.7$ K and $\Delta V = 10.0$ km s^{-1}, respectively.

Two sets of radiative transfer calculations were provided. First, we used the available rate coefficients from the LAMDA data base (Schöier et al. 2005). This data base contains scaled *ortho*- and *para*-NH_3 rate coefficients in collision with H_2 at 100 K kinetic temperature to estimate the H_3O^+–H_2 collisional rates based on the data from Offer & van Hemert 1992. The LAMDA data base provides such rates for 36 de-excitation transitions in case of *ortho*- and 91 transitions in case of *para*-H_3O^+.

In the second set of radiative transfer calculations, we used the new rate coefficients, which were calculated according to the method discussed in subsection 2.2. We have explicitly taken into account the rate coefficients between 10 and 100 K kinetic temperatures for 55 transitions in case of *ortho*- and 180 transitions in case of *para*-H_3O^+. For both sets of calculations, the rotational energies along with the radiative transition frequencies and Einstein *A*-coefficients were used as it is proposed in JPL data base (Pickett et al. 2010, Species Tag: 19004, version 3, compiled by Yu & Drouin, Jan. 2010). In total 11 rotational states (up to the $j_k^\epsilon = 5_3^+$ state) were included in the analysis of *ortho*-H_3O^+, while in case of *para*-H_3O^+, we considered the 20 lowest states (including the $j_k^\epsilon = 5_4^-$ state as the highest, see Table. 1 for more details).

3 RESULTS AND DISCUSSION

3.1 Rotational de-excitation cross sections

Figs 1 and 2 show the collisional energy dependence of some selected de-excitation cross sections for *o*-H_3O^+ and *p*-H_3O^+ collision with *p*-H_2, respectively. We compare our data with the corresponding cross

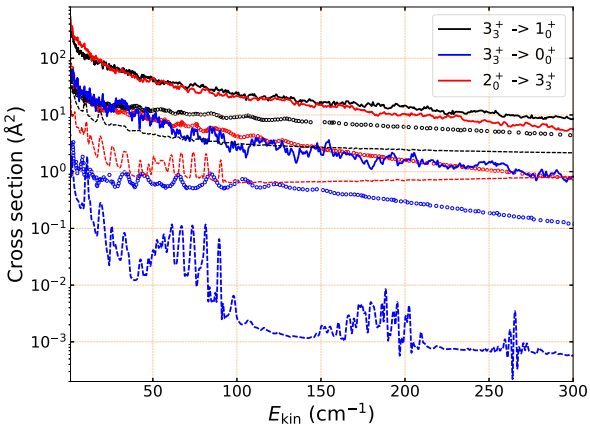

Figure 1. Rotational de-excitation cross sections for some selected transitions in collision of *o*-H_3O^+ with *p*-H_2. Our results (solid lines) are compared with the corresponding data of Bouhafs et al. (2017) (*o*-NH_3 – *p*-H_2, dashed lines) and El Hanini et al. (2019) (*o*-H_3O^+ – He, circles). Identical colours indicate identical transitions.

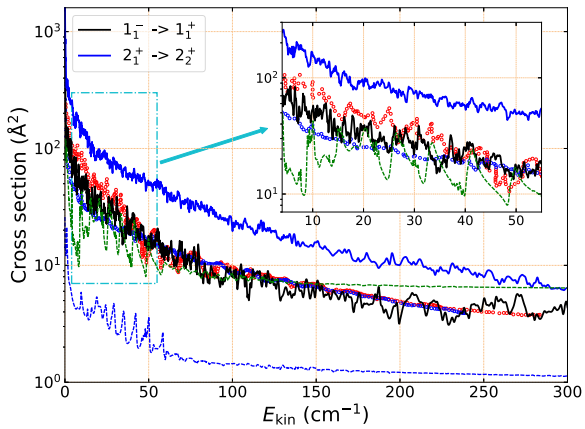

Figure 2. Rotational de-excitation cross sections for some selected transitions in collision of *p*-H_3O^+ with *p*-H_2. Our results (solid lines) are compared with the corresponding data of Bouhafs et al. (2017) (*p*-NH_3 – *p*-H_2, dashed lines) and El Hanini et al. (2019) (*p*-H_3O^+ – He, circles). The blue lines and circles are for the $2_1^+ \rightarrow 2_2^+$ transition, while both the green dashed line and the red circles show the data for $1_1^- \rightarrow 1_1^+$ transition.

sections for H_3O^+–He (El Hanini et al. 2019) and NH_3–H_2 (Bouhafs et al. 2017) collisions. The reason why we perform a comparative analysis also with ammonia data is because NH_3 was assumed to be a template for the collisions with H_3O^+ (see for example Offer & van Hemert 1992 for details). It is worth mentioning, however, that the labelling of the rotational levels in both of the referred works is somewhat different from those we calculated for the hydronium cation (see Table. 1). The source of such differences is obvious in comparison with NH_3, however, the incorrect structure of rotational levels for H_3O^+ is because the large inversion splitting constant of the cation is neglected in the calculations of El Hanini et al. (2019).

Offer & van Hemert (1992) only calculated excitation cross sections and only for one single energy both for *para*- and *ortho*-H_3O^+ collision with H_2. These cross sections were calculated in the low-energy region (at 101 and 145 cm^{-1}, respectively), where the resonances are very dominant, and their structure and amplitude strongly depend on the quality of the potential used for the calculations. We compared the state-to-state cross sections with the corresponding data of Offer & van Hemert (1992), and we found that our results usually highly overestimates them (up to 1 or even 2 orders of magnitude). It is important to mention also that in order to make a comparison of the de-excitation cross sections directly in Figs 1 and 2, an analytical conversion is needed. This conversion involves the k_j^2 (wavevector) parameter, which linearly depends on the difference between the total collision energy and the rotational energy of the particular states involved in the transition. Since the quality of the conversion is sensitive to the rotational level energy (especially in case of higher states), which are not listed precisely in the work of Offer & van Hemert (1992; see fig. 3 therein), it is not possible to guarantee a good accuracy for the conversion. Because of the mentioned reasons, we decided not to include the results of Offer & van Hemert (1992) in our global analysis.

In the case of *o*-H_3O^+ collision with *p*-H_2, we selected some transitions with $\Delta j = 1{-}3$ and $\Delta k = 3$. As one can see there is a significant difference between our results and the cross sections of both El Hanini et al. (2019) and Bouhafs et al. (2017) in the whole kinetic energy range considered. Typically our cross sections are about an order of magnitude larger than the corresponding data from the literature. The relative difference is the smallest in case of the $3_3^+ \rightarrow 1_0^+$ transition, and somewhat decreases with increasing energy. For other transitions, the difference is relatively constant and does not depend strongly on energy, except in the case of the $2_0^+ \rightarrow 3_3^+$ transition in comparison with the NH_3 data. Significantly there is no constant linear scaling between our data and those of El Hanini et al. (2019) or Bouhafs et al. (2017), which confirms the relevance of the new calculations. As one can see also in Fig. 1, another important difference is that the new cross sections are characterized by a dense resonance structure, which is also contrary to the previously published data. This is certainly due to the very large differences between the well depths of the interaction potential. While for the H_3O^+–He system, it is about 354.53 cm^{-1}(El Hanini et al. 2019) and for the NH_3–H_2 complex, it is 267 cm^{-1}(Bouhafs et al. 2017), the well depth of the PES in our calculation is 5–7 times larger, about 1887.2 cm^{-1}.

In order to analyse the cross sections for *p*-H_3O^+ – *p*–H_2 collision (see Fig. 2) we selected only two transitions (both with $\Delta j = 0$). The solid black line shows our cross sections for the $1_1^- \rightarrow 1_1^+$ inversion transition, while the solid blue line refers to $2_1^+ \rightarrow 2_2^+$. The results are compared with the corresponding data for *p*-H_3O^+ – He (El Hanini et al. 2019) and *p*-NH_3 – *p*-H_2 (Bouhafs et al. 2017) collisions. The observed relative differences are significantly smaller for the transition within $j = 1$, but still very large for the $j = 2$ transition. The strong resonance structures in the cross sections are significant for this type of collisions as well. The differences are mainly due to these resonances in the case of $1_1^- \rightarrow 1_1^+$ transition, while for the $2_1^+ \rightarrow 2_2^+$ process a larger relative difference is observed, from a factor of 2 up to more than an order of magnitude.

In Fig. 3, we compare the cross sections for all the possible low-frequency transitions ($\nu_{i \rightarrow f} < 1000$ GHz) up to 500 cm^{-1}collision energies. Transitions both for *o*-H_3O^+ and *p*-H_3O^+ nuclear spin isomers were considered, for which we also present radiative transfer calculations later (see subsection 3.3). The σ do not deviate strongly, the maximal difference between them is within a factor of 3. It is not surprising that the largest cross sections are calculated for the case of $0_0^- \rightarrow 1_0^+$ transition into the ground state. As one can see, all σ are characterized with a very strong resonance behaviour, which indicates that a very dense sampling of collision energy (with a step size $E_{step} \sim 0.1$ cm^{-1}) is required to adequately compute

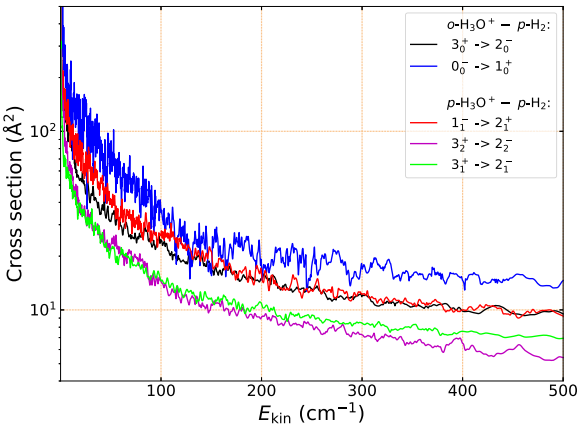

Figure 3. Rotational de-excitation cross sections for the low-frequency (ν < 1000 GHz) transitions in o-H_3O^+ and p-H_3O^+ collisions with p-H_2.

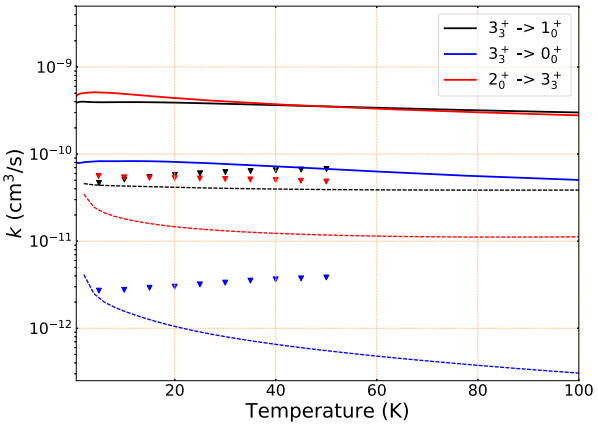

Figure 4. Kinetic temperature dependence of the rate coefficients for some selected rotational transitions in collision of o-H_3O^+ with p-H_2. Our results (solid lines) are compared with the corresponding data of Bouhafs et al. (2017) (o-NH_3 – p-H_2, dashed lines) and El Hanini et al. (2019) (o-H_3O^+ – He, triangles). Identical colours indicate identical transitions.

the corresponding rate coefficients (especially below 300–400 cm^{-1}, where the resonances are the strongest).

3.2 Rate coefficients

Once the state-to-state cross sections were calculated, we computed the corresponding rate coefficients for the H_3O^+–H_2 collision (see subsection 2.2 for details). In Fig. 4, the rate coefficients for the o-H_3O^+ − p-H_2 collision are compared with the available data from the literature for the same transitions presented in Fig. 1. The large difference between our results and the collisional rates of both El Hanini et al. (2019) and Bouhafs et al. (2017) is even more visible in this plot in the whole temperature range (i.e. up to T_{kin} = 100 K). The smaller deviation is observed for the $3_3^+ \rightarrow 1_0^+$ transition (one order of magnitude compared to two orders of magnitude for the other transition). In general, the relative difference between the corresponding $k(T)$ is smaller for higher absolute rate coefficient values. It is worth noting also that there is no direct scaling (i.e. linear dependence) observed between the rate coefficients compared in Fig. 4 with respect to kinetic temperature change.

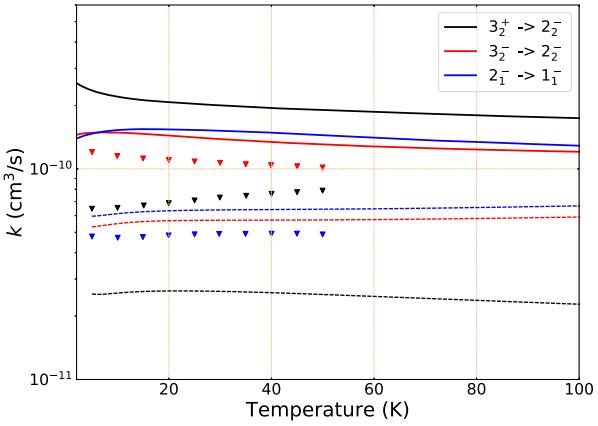

Figure 5. Kinetic temperature dependence of the rate coefficients for some selected rotational transitions in collision of p-H_3O^+ with p-H_2. Our results (solid lines) are compared with the corresponding data of Bouhafs et al. (2017) (p-NH_3 – p-H_2, dashed lines) and El Hanini et al. (2019) (p-H_3O^+ – He, triangles). Identical colours indicate identical transitions.

As it is expected, the relative difference between the calculated $k(T)$ for p-H_3O^+ − p–H_2 collision and the corresponding data from the literature (Bouhafs et al. 2017; El Hanini et al. 2019) is similar to those for the o-H_3O^+ − p-H_2 process. Fig. 5 shows the temperature dependence of the p-H_3O^+ − p–H_2 thermal rate coefficients for some selected transitions, compared with the previously published data. It is worth mentioning, however, that we selected different states from those shown in Fig. 2, because of the lack of collisional rate coefficients in the literature for those transitions. The magnitude of deviations does not depend clearly on the absolute value of the rates, however, it is rather small (from about 20 per cent up to about a factor of 2) in the case of the $3_2^- \rightarrow 2_2^-$ transition, which is the lowest by the amplitude in our calculations. While our results show a rather strong resemblance for the $3_2^- \rightarrow 2_2^-$ and $2_1^- \rightarrow 1_1^-$ transitions, this is not the case with the corresponding data of El Hanini et al. (2019). The rate coefficients for these transitions in the work of Bouhafs et al. (2017) also show a strong correlation, but our results are significantly larger (by about a factor of 2). The largest differences (up to an order of magnitude) are found for the $3_2^+ \rightarrow 2_2^-$ de-excitation process as compared with the results of Bouhafs et al. (2017) for NH_3.

Fig. 6 compares the de-excitation rates for the same low-frequency transitions studied in Fig. 3. Both the o-H_3O^+ and p-H_3O^+ nuclear spin isomers were considered again. One can see that the absolute difference between the $k(T)$ varies from some per cents up to a factor of 3. It is worth mentioning again that the dependence of the rate coefficients on the temperature is not uniform, which is especially significant at lower T_{kin}. Above 60 K, the rate coefficients decrease rather monotonically, and a constant scaling factor between them could be easily derived for this temperature region.

After analysing all the state-to-state rate coefficients, some important conclusion could be drawn. In the 10 to 100 K interval, the temperature dependence is not strong, which is in accordance with the Langevin capture model. Above 40–50 K, all the rate coefficients are monotonically decreasing with temperature, which allows one to use simple extrapolation methods towards higher kinetic temperatures, however, the precision of such extrapolations are questionable.

In order to demonstrate the importance of new rate coefficients in the potential astrophysical applications, we compare our results with the most recent $k(T)$ listed in the LAMDA data base (Schöier et al. 2005). Currently, these rate coefficients are used for the radiative transfer modelling, which involves hydronium. The ratios

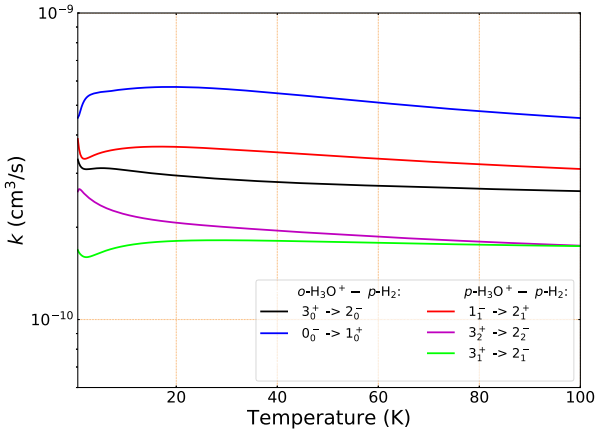

Figure 6. Kinetic temperature dependence of the rate coefficients for the low-frequency (υ < 1000 GHz) transitions in both o-H_3O^+ and p-H_3O^+ collisions with p-H_2.

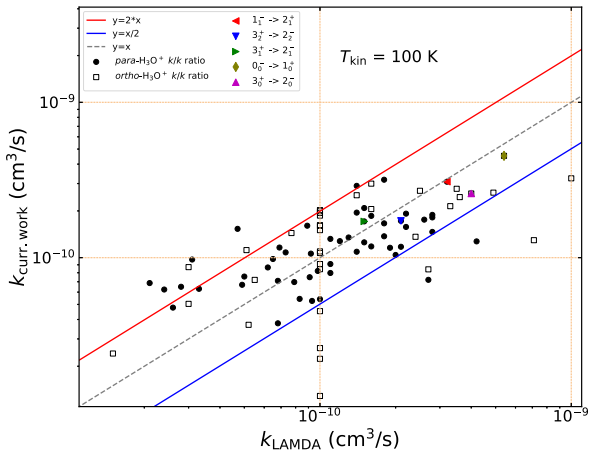

Figure 7. State-to-state ratios of our recent thermal rate coefficients and the corresponding data listed in the LAMDA data base (Schöier et al. 2005). The corresponding data both for o-H_3O^+ and p-H_3O^+ are considered at 100 K kinetic temperature.

of the collisional rate coefficients both for o-H_3O^+ and p-H_3O^+ are shown in Fig. 7 at 100 K kinetic temperature. As one can see, the $k(T)$ do not correlate well, i.e. no linear scaling from the data of LAMDA data base to our new rates can be found. In general, the ratio varies between factors of 0.5 and 2 (except for some o-H_3O^+ transitions) and no significant difference can be found for *ortho* and *para* nuclear symmetries. For most of the transitions, the following tendency is valid: as the magnitude of the $k(T)$ is increasing, their relative ratio is decreasing. In comparison with the data from the literature, our rates are higher for the low-magnitude transitions (up to about 2×10^{-10} cm^3 s^{-1}), while for higher rates, they are lower. We would like to emphasize again that due to this non-linearity, the new collisional rate coefficients are important for adequate modelling of hydronium in astrophysical media.

The corresponding ratios for the low-frequency transitions are highlighted with alternative colours. While the LAMDA data base currently contains only collisional data at 100 K, it is important to provide temperature-dependent rate coefficients as well, since their amplitude can vary (decrease) with increasing T_{kin}.

3.3 Excitation of H_3O^+ in low-temperature interstellar regions

In order to estimate the impact of our new collisional data on the astrophysical observables, we have computed the excitation of both *ortho*- and *para*-H_3O^+ using the large velocity gradient RADEX non-LTE radiative transfer computer programme (see Subsection 2.3 for details). We have used the rate coefficients computed for collision with p-H_2, presented in the previous section. For comparison, we provided the same radiative transfer calculations using the corresponding $k(T)$ data from the LAMDA data base (Schöier et al. 2005). The radiance (brightness) temperatures for the $1_1^- \rightarrow 2_1^+$, $3_2^+ \rightarrow 2_2^-$ and $3_0^+ \rightarrow 2_0^-$ transitions are compared with the results of Phillips et al. (1992; see Fig. 8). The latter de-excitation processes are characterized with 307.2, 364.8, and 396.3 GHz transition frequencies, respectively (see Fig. 3 for the corresponding cross sections and Fig. 6 for the rate coefficients).

First, we analysed the optical depth (τ) for these transitions at $N = 10^{15}$ cm^{-2} column density. We found that all the four transitions are optically 'thin', since we found very low τ values for them under strict LTE-conditions (above 10^9 cm^{-3} hydrogen densities):

(i) $\tau \approx 0.2-0.22$ for the $3_0^+ \rightarrow 2_0^-$ transition (396.3 GHz),
(ii) $\tau \approx 0.15-0.17$ for the $1_1^- \rightarrow 2_1^+$ transition (307.2 GHz),
(iii) $\tau \approx 0.08-0.1$ for the $3_2^+ \rightarrow 2_2^-$ transition (364.8 GHz),

where the two τ-values refer to results obtained using our new $k(T)$ data and those of from the LAMDA data base (Schöier et al. 2005), respectively. At lower H_2 densities (below 10^6 cm^{-3}), the calculated optical depth values are lower (<0.1), except of the $1_1^- \rightarrow 2_1^+$ (307.2 GHz) transition, for which $\tau \approx 1$ between 10^3-10^4 cm^{-3} H_2 densities.

Fig. 8 shows the dependence of T_R radiance temperature on $n(H_2)$ gas density for the above mentioned transitions. We analysed this dependence for different N column densities ranging from 1×10^{12} up to 1×10^{15} cm^{-2} at 50 and 100 K gas temperatures. As one can see, there is a good qualitative agreement between the calculated radiance temperatures using our new rate coefficients and those listed by Phillips et al. (1992) for the whole molecular density range. However, while analysing the results obtained using the LAMDA rate coefficients, we observe some deviations. These deviations with respect to the results obtained with our $k(T)$ data are ranging from some per cents up to a factor of 2 (compare the solid and dash–dotted curves on Fig. 8). As one can expect, the deviations are more significant under non-LTE conditions, i.e. below 10^6 cm^{-3} hydrogen densities, where they strongly depend both on T_{kin} as well as on the type of the transition. It is worth mentioning, however, that at 100 K, slight differences (up to about 10 per cent) are observed also at high H_2 densities, where the collisional rates do not contribute in the modelling. These differences can be explained by the different number of rotational levels and transitions involved in the two sets of radiative transfer calculations. Thus, in the modelling with our rate coefficients, the collisional data for the lowest 20 and 11 rotational states are included for the *para*- and *ortho*-H_3O^+, respectively. At the same time, in the modelling with the LAMDA rate coefficients, the corresponding data are available only for the lowest 14 and 9 rotational levels, respectively. As one can see, at lower temperatures (i.e. at 50 K), these differences do not lead to large discrepancies between the two calculations, however, at 100 K, the additional rotational states have significant impact on the results. We found that the disagreement between the two calculated set of T_R is the largest in the case of $3_0^+ \rightarrow 2_0^-$ o-H_3O^+ – p-H_2 transition and is stronger at higher kinetic temperature. It does not depend, however, on the column density. The observed threshold (i.e. the critical density) to

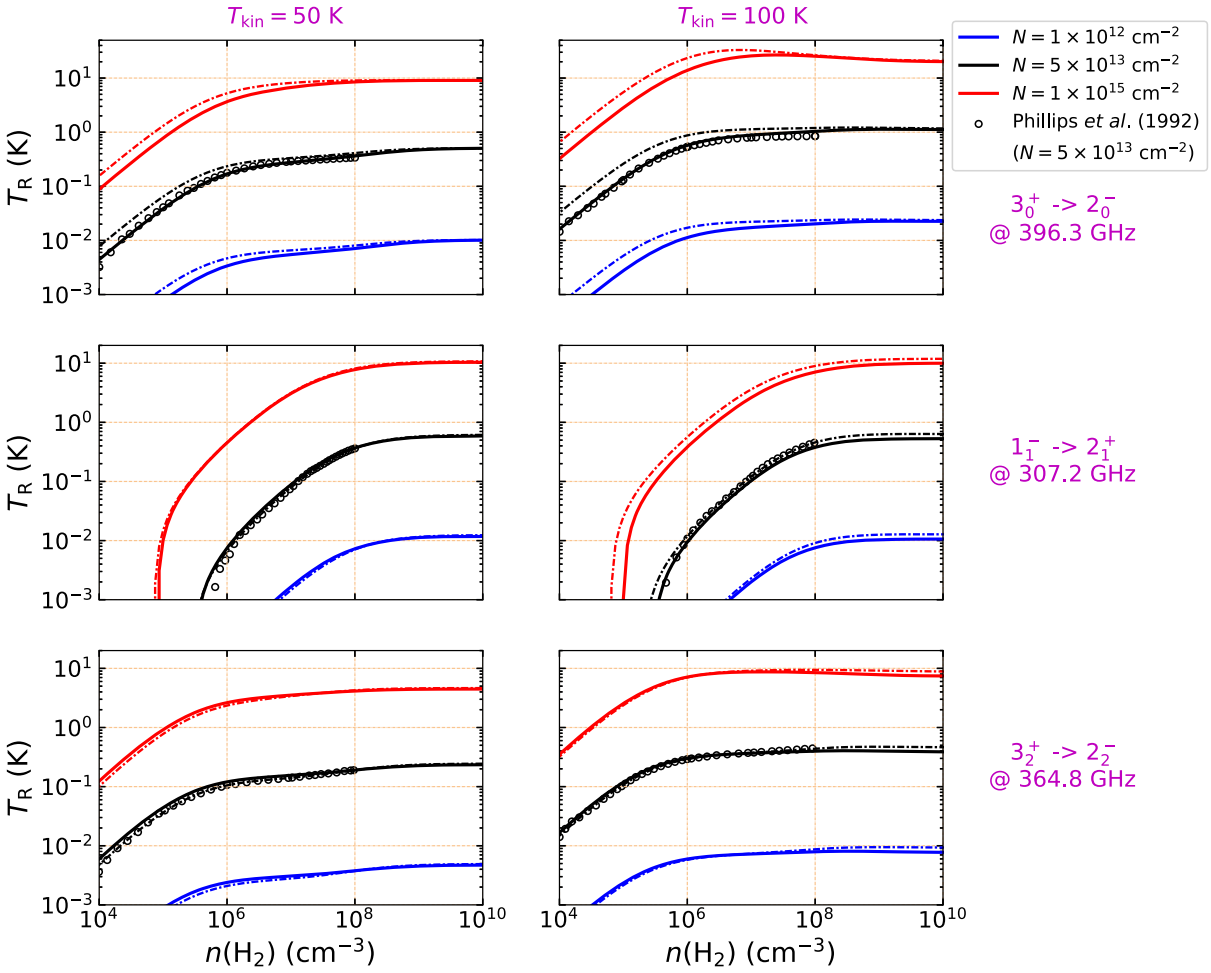

Figure 8. T_R radiance temperatures for the H_3O^+ cation's 307, 365, and 396 GHz lines as a function of $n(H_2)$ molecular density, computed using the rate coefficients from the LAMDA data base (dash–dotted lines; Schöier et al. 2005) and those from this paper (solid lines). The three panels on the left-hand side represent the results at 50 K kinetic temperature for the three transitions studied, while on the right-hand side panels, the results at 100 K are shown. The different colours of the subplots denote different column densities, ranging from $N = 10^{12}$ up to $N = 10^{15}$ cm^{-2}.

reach LTE conditions is about 10^8 cm^{-3} H_2 density for all considered de-excitation processes.

To further study the effect of the new rate coefficients on the radiative transfer models, we provide also a comparative analysis for the T_{exc} excitation temperatures. In Fig. 9, one can see the dependence of T_{exc} on H_2 molecular density in case of some low-frequency transitions, for which population inversion effects were observed. In particular, the $3_0^+ \rightarrow 2_0^-$, $3_1^+ \rightarrow 2_1^-$ and $3_2^+ \rightarrow 2_2^-$ de-excitation processes were considered with 396.3, 388.5, and 364.8 GHz transition frequencies, respectively. In the subplots of Fig. 9, we compared again two sets of results, which are obtained using our new $k(T)$ and those from the LAMDA data base. Analogously to the previous case, we have analysed the results for column densities between 1×10^{12} and 1×10^{15} cm^{-2} at 50 and 100 K kinetic temperatures. Unfortunately, for these quantities, we could not find any available data in the literature. For better visualization, the plots show the logarithm of the excitation temperatures multiplied by ε , where $\varepsilon = 1$ for positive and $\varepsilon = -1$ for negative T_{exc} values, respectively. As one can see for all three transitions under consideration, the population inversion is observed in a very broad gas density range, starting from low $n(H_2)$ densities (below 10^4 cm^{-3}). The width of this region strongly depends both on the column density and the kinetic temperature. Between 10^8 and 10^9 cm^{-3} however, i.e. around the threshold to reach strict LTE-conditions, the population inversion is quenched, and at high densities there are almost no differences between the two sets of data. On the other hand, while we compare the results for the particular transitions under the same physical conditions, which were obtained with the two sets of rates (see the solid and dash–dotted curves in Fig. 9), we find significant differences. First, there is a rather large shift in the critical density region, where T_{exc} change sign from '$-$' to '$+$'. This shift is varying between some per cents and about a factor of 2. Slight deviations are also observed in the amplitudes of excitation temperatures near these turning points. These deviations are usually higher in case of larger column densities and lower kinetic temperatures, for which we observe differences as high as an order of magnitude (see for example the $3_1^+ \rightarrow 2_1^-$ and $3_2^+ \rightarrow 2_2^-$ transitions at 50 K). It is also important to note that the minimal and maximal amplitudes in the critical density region are very close for all of the studied transitions and do not depend strongly on the particular physical conditions. Aalto and coworkers showed earlier (Aalto et al. 2011) that the results of radiative transfer calculations are also sensitive to the adopted background temperature. So for a reliable interpretation of observations, the T_{bg} value should be chosen carefully.

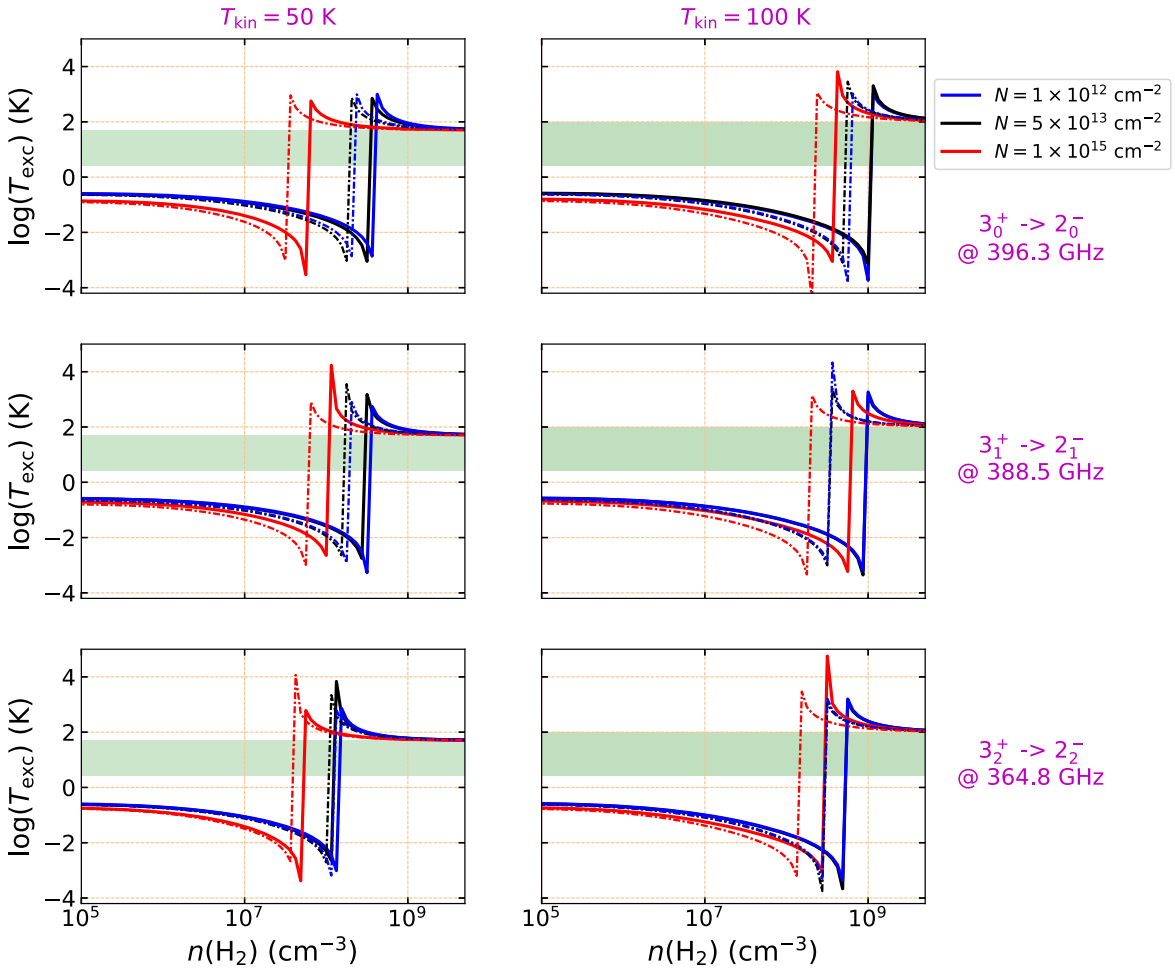

Figure 9. Logarithm of the excitation temperatures log (T_{exc}) for the H_3O^+ cation's 365, 389, and 396 GHz emission lines as a function of $n(H_2)$ molecular density, computed using the rate coefficients from the LAMDA data base (dash–dotted lines; Schöier et al. 2005) and those from this paper (solid lines). The values at the ordinate are multiplied by a factor $\varepsilon = \pm 1$, the sign of which corresponds to the sign of T_{exc}. The green horizontal area defines the interval of temperatures ranging from $T_{bg} = 2.7$ K up to T_{kin}. The definition and parameters used in the individual panels are identical to those of in Fig. 8.

4 CONCLUSIONS

We have presented state-to-state rotational de-excitation cross sections and thermal rate coefficients for collisions of *ortho*-H_3O^+ and *para*-H_3O^+ with *p*-H_2, which is one of the most abundant colliders in interstellar clouds. The theoretical calculations are performed within an accurate close-coupling formalism. Our recent, explicitly correlated 5D rigid-rotor PES (Paper I) was used for collisional dynamics studies. A broad kinetic energy range was considered (<800 cm^{-1}), which allowed one to calculate the corresponding state-to-state rate coefficients up to 100 K temperature. Since accurate data for the studied collisional system is missing in the literature, we compare our results with the corresponding data for the isoelectronic H_3O^+–He (El Hanini et al. 2019) and NH_3–H_2 (Bouhafs et al. 2017) collisions. In most cases, significant differences are observed (as high as an order of magnitude) both for the cross sections and rate coefficients, where our new data are notably larger than the corresponding data from the literature in case of the analysed de-excitation processes. We also compared the rate coefficients for the individual rotational transitions with the most recent data provided in the LAMDA data base (Schöier et al. 2005). The deviations are rather large, usually within a factor of 2. It is also worth mentioning that no general, linear scaling rule could be established to find a correspondence between the literature data and those of our recent work. Based on these findings, we can conclude that the new collisional rates are obviously important and allows one a more adequate modelling of hydronium observations in astrophysical media.

In order to investigate the effect of the new rate coefficients on the excitation of *ortho*-H_3O^+ and *para*-H_3O^+, we have computed the excitation of these species using a non-LTE radiative transfer code under various physical conditions that are typical of molecular clouds. As the comparison with the results obtained from LAMDA rate coefficients has shown, our new collisional data have a significant, non-negligible impact on the astrophysical observables in such models. This effect on the excitation of hydronium is more remarkable at lower hydrogen densities, where the LTE-conditions are not fulfilled. It is worth mentioning, however, that some discrepancies for the radiance temperatures were found also under strict LTE-conditions. These discrepancies are due to the fact that our new collisional data involve more rotational levels compared to the LAMDA data base, which can significantly contribute to the radiative transfer models at higher temperatures. The column densities of H_3O^+ in interstellar clouds, thus, should be revisited based on the new collisional data. This can be used then as an indirect way for more precise estimates

of the gas-phase formation of O_2 and H_2O molecules in the ISM, since these species primarily formed by dissociative recombination of hydronium cations.

It is also important to note that the calculated rate coefficients slightly depend on the kinetic temperature. Nevertheless, for more precise astrophysical applications, especially to study warmer astronomical regions (with temperatures around 250−300 K), it is required to extend the collisional energy and kinetic temperature range. For this reason, our future studies will be addressed to the excitation of H_3O^+ at higher temperatures, considering rotational cross sections up to 1500–1600 cm^{-1}collision energies. In addition, since it is crucial in the high-temperature regions of the ISM, we will extend our calculations also for collisional processes involving *ortho*-H_2.

ACKNOWLEDGEMENTS

We acknowledge financial support from the European Research Council (Consolidator Grant COLLEXISM, Grant Agreement No. 811363) and the Programme National 'Physique et Chimie du Milieu Interstellaire' (PCMI) of CNRS/INSU with INC/INP cofunded by CEA and CNES. We wish to acknowledge the support from the CINES/GENCI for awarding us access to the OCCIGEN supercomputer within the A0070411036 project as well as the GRICAD infrastructure (https://gricad.univ-grenoble-alpes.fr), which is supported by Grenoble research communities. We also acknowledge KIFÜ for awarding us access to HPC resources based in Hungary. FL acknowledges the Institut Universitaire de France.

DATA AVAILABILITY STATEMENT

The data underlying this article will be shared on reasonable request to the corresponding author.

REFERENCES

Aalto S., Costagliola F., van der Tak F., Meijerink R., 2011, A&A, 527, A69
Alexander M. H., Manolopoulos D. E., 1987, J. Chem. Phys., 86, 2044
Bouhafs N., Rist C., Daniel F., Dumouchel F., Lique F., Wiesenfeld L., Faure A., 2017, MNRAS, 470, 2204
Boys S. F., Bernardi F., 1970, Mol. Phys., 19, 553
Bubin S., Adamowicz L., 2003, J. Chem. Phys., 118, 3079
Demes S., Lique F., Faure A., Rist C., 2020, J. Chem. Phys., 153, 094301(Paper I)
El Hanini H., Najar F., Naouai M., Jaidane N. E., 2019, Physic. Chemist. Chem. Phys., 21, 11705
Faure A., Tennyson J., 2003, MNRAS, 340, 468
Gerin M. et al., 2010, A&A, 518, 1
Goicoechea J. R., Cernicharo J., 2001, ApJ, 554, L213
González-Alfonso E. et al., 2013, A&A, 550, A25
Herbst E., Klemperer W., 1973, ApJ, 185, 505
Hollenbach D., Kaufman M. J., Neufeld D., Wolfire M., Goicoechea J. R., 2012, ApJ, 754, 105
Indriolo N. et al., 2015, ApJ, 800, 40
Jensen M. J., Bilodeau R. C., Safvan C. P., Seiersen K., Andersen L. H., Pedersen H. B., Heber O., 2000, ApJ, 543, 764
Le Picard S., Biennier L., Monnerville M., Guo H., 2019, 2514–3433, Gas-Phase Chemistry in Space, IoP Publishing, Bristol, p. 3
Mann J. E., Xie Z., Savee J. D., Bowman J. M., Continetti R. E., 2013, J. Physic. Chemist. A, 117, 7256
Manolopoulos D. E., 1986, J. Chem. Phys., 85, 6425
Offer A. R., van Hemert M. C., 1992, Chem. Phys., 163, 83
Phillips T. G., van Dishoeck E. F., Keene J., 1992, ApJ, 399, 533
Pickett H. M., Cohen E. A., Drouin B. J., 2010, J. Quant. Spectrosc. Radiat. Transf., 111, 1617
Rist C., Faure A., 2012, J. Math. Chem., 50, 588
Rist C., Alexander M. H., Valiron P., 1993, J. Chem. Phys., 98, 4662
Roueff E., Lique F., 2013, Chem. Rev., 113, 8906
Schöier F. L., Van Der Tak F. F., Van Dishoeck E. F., Black J. H., 2005, A&A., 432, 369
Sternberg A., Dalgarno A., 1995, ApJSS, 99, 565
Tang J., Oka T., 1999, J. Mol. Spectr., 196, 120
Valiron P., Wernli M., Faure A., Wiesenfeld L., Rist C., Kedžuch S., Noga J., 2008, J. Chem. Phys., 129, 134306
van der Tak F. F., Van Dishoeck E. F., 2000, A&A., 358, 79
van der Tak F. F. S., Black J. H., Schöier F. L., Jansen D. J., van Dishoeck E. F., 2007, A&A., 468, 627
van der Tak F. F. S., Aalto S., Meijerink R., 2008, A&A, 477, L5
van der Tak F. F. A. W., Liu L., Güsten R., 2016, A&A, 593, A43
van der Tak F. F. S., Lique F., Faure A., Black J. H., van Dishoeck E. F., 2020, Atoms, 8, 15
van Dishoeck E. F., Herbst E., Neufeld D. A., 2013, Chem. Rev., 113, 9043
Vejby-Christensen L., Andersen L. H., Heber O., Kella D., Pedersen H. B., Schmidt H. T., Zajfman D., 1997, ApJ, 483, 531
Yu Q., Bowman J. M., 2016, J. Chem. Theory Comput., 12, 5284
Yu S., Drouin B. J., Pearson J. C., Pickett H. M., 2009, ApJSS, 180, 119
Yurchenko S. N., Tennyson J., Miller S., Melnikov V. V., O'Donoghue J., Moore L., 2020, MNRAS, 497, 2340
Zhaunerchyk V. et al., 2009, J. Chem. Phys., 130, 214302

SUPPORTING INFORMATION

Supplementary data are available at *MNRAS* online.

supplementary-RADEX_molecular_data_files.zip

The RADEX-compatible molecular data files, which are used in the radiative transfer calculations, and which include the particular state-to-state rate coefficient data for *ortho*- and *para*-H_3O^+ collisions with *para*-H_2 up to 100 K, are provided as supplementary material.

Please note: Oxford University Press is not responsible for the content or functionality of any supporting materials supplied by the authors. Any queries (other than missing material) should be directed to the corresponding author for the article.

This paper has been typeset from a TEX/LATEX file prepared by the author.